VOL. 11, NO. 21, NOVEMBER 2016 ISSN 1819-6608
ARPN Journal of Engineering and Applied Sciences

www.arpnjournals.com

SIMULATION OF ROCK SHEAR FRACTURE IN THE CASE OF DIFFERENT INCLINED NOTCHES

S. J. Jung[1] and A. M. Abu Abdo[2]
[1]Department of Civil Engineering, University of Idaho, Moscow, United States of America
[2]Department of Civil and Infrastructure Engineering American University of Ras Al Khaimah Ras Al Khaimah, United Arab Emirates
E-Mail: sjung@uidaho.edu

ABSTRACT

Understanding Rock Fracture mechanism is essential in civil engineering applications. Failure due to shear strength is considered the main cause for rock failure. This study was conducted to evaluate shear strength of rock (Sandstone) specimens with different notch inclinations (10º, 20º, 30º, 35º and 40º) under pure shear testing. Finite Element simulations were used to determine stresses in tested Sandstone specimens with different notch angles. Results of the simulations were utilized in Mohr envelope form of power law (n-type) to investigate shear failure mechanism in rock and prediction of crack propagation pattern. It was found that the stress state in term of τ-σ curve from Finite Element simulation results and the Mohr-type envelope could explain the failure mechanism in Sandstone and the crack propagation pattern in tested specimens with relation to different notches inclination degrees. Furthermore, it was found that the tensile strength of Sandstone was needed to have a better control to the right end of the Mohr-type envelopes, which could be used to analyze and understand more about the mechanism of the steady and curving crack propagation of the sandstone specimen with big d/H ration.

Keywords: rock mechanics, shear strength, fracture, shear failure, inclined notch, modeling, finite element analysis, mohr-type envelop, sandstone.

1. INTRODUCTION

Understanding failure and fracture mechanism in Rock is essential in civil engineering applications, especially when it comes to Rock burst, rock cutting, hydro-fracturing, and explosive fracturing. Many believes that shear failure is the main reason for rock failure, which caused considerable confusion among researchers [1]. Multiple studies were conducted to understand and develop different methods for determining shear failure and crack propagation in rocks [1-11].With advances in modeling and computer simulations, many researchers investigated shear failure in rocks using numerical approaches and validated their modeling results with experimental results. The most commonly used and successful methods were Finite Element Method (FEM) and Discrete Element Method (DEM) [12].

Matsui and San [13] conducted a study to verify shear strength reduction technique using Finite Element slope stability analysis. They argued that the proposed method was applicable to practical designs, since results were in agreement with field test data and onsite observations. Jung *et al.* [7] conducted various simulations on shear strength testing of rock specimens with vertical and inclined notches via Finite Element simulations. Results showed that Finite Element simulations assisted in the prediction and understanding of crack behavior and pattern in rock failures. Later, Li *et al*. [14] utilized Finite Element simulations in slope stability analysis by adopting nonlinear shear strength criteria of power-law type model. The study concluded that Finite Element analysis was better than other methods, since there was no need to assume a prior failure mechanism. In 2013, a study was conducted to investigate the stability of the rock slope under Jinsha River Bridge foundation in China. Analysis was conducted using Finite Element method and results indicated that there was a potential shear failure region in the rock mass under the main pier. Based on their findings, strengthen of the foundation was recommended to prevent the slope failure under external forces [15].

The accuracy of Finite Element analysis depends largely on the numerical models simulating element properties and boundary conditions (material properties). Stead *et al.* [16] presented three developments in the classification of complex rock slope deformation and failure using numerical techniques. Three levels of sophistication were developed and demonstrated. Li *et al.* [17] evaluated Mohr-Coulomb strength theory, Griffith strength theory and Hoek-Brown criterion with the brittle-shear coupled strength model. Results showed strong correlation between test data and numerical models results. In a later study, a theoretical analysis was conducted for analyzing brittle shear failure of rocks. Mohr-Coulomb strength theory, Griffith strength theory and Hoek-Brown criterion with the brittle-shear strength model were adopted in the analysis. Mixed granite in Shuichang slope strength analysis was conducted using the brittle shear failure model; analysis results were consistent with the experimental data [18].

2. STUDY OBJECTIVES

To investigate shear failure mechanism in rock and prediction of crack propagation pattern this study was conducted. Thus, the objectives of this study were as follow:

a) Enhance the understanding of the shear failure mechanism in rock.
b) Evaluate the effects of different notch degrees in tested specimens on shear failure of Sandstone and crack propagation.

c) Investigate the effectiveness of Mohr envelope form of power law (n-type) in shear failure mechanism in Sandstone and prediction of crack propagation pattern.

3. EXPERIMENTAL PROGRAM

In previous studies [1, 7, 8] shear fracture of sandstone specimens with different inclined notches were investigated. Figure 1 shows the geometry and loading configuration of a tested specimen. All tested specimens had an identical d(1.9 cm) and d to H ratio (0.19). However, the slant notch angle varied between specimens (10º, 20º, 30º, 35º and 40º). All tested specimens with different slant notches broke instantly and vertically. A close observation indicated that the crack in tested specimens with vertical notches did not go through the two notch tips and the propagation path was roughly like an 'S' shape. Tested specimens with 10º and 20º slant notch cases had a fracture pattern of a polyline jointed by two line, while the crack propagated undeviatingly to pass through the two notch tips and follow the middle line straightly for specimens with 30º and 40º slant notches. A straighter crack was created in specimens with 30º to 40º inclined notches than the crack in specimens with both vertical notches and other slant notches of 10º and 20º.

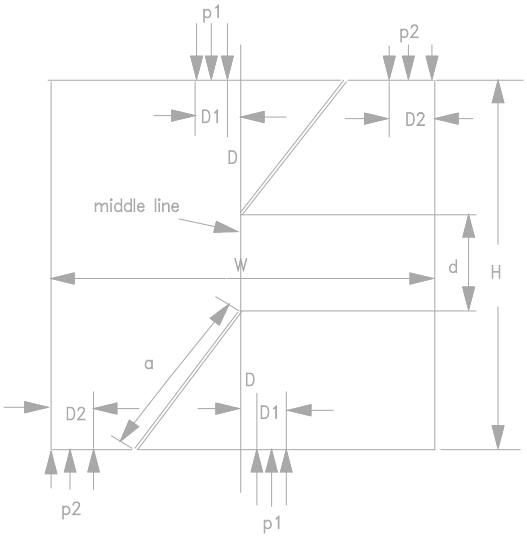

Figure-1. Specimen geometry and loading configuration (After [1]).

Table-1 lists the experimental data and Figure-2 shows the relationship between the failure load and the corresponding slant notches. Those experimental data demonstrate that as the slant notch degree increased from 0º to 35º, the failure load P_{max} increased from 3883N to 6212N, and so did the average shear strength. As for the 35º to 40º slant notch degrees, the load P_{max} decreased to 6144N.

Table-1. Failure load of sandstone specimen with slant notches.

Degree Type	**a** (cm)	**d** (cm)	**T** (cm)	**Area=d*T** (cm^2)	**Failure load** (N)	**Strength** (kPa)
0º	4.05	1.9	7.0	13.3	3883	2870
10º	4.11	1.9	7.0	13.3	4851	3585
20º	4.31	1.9	7.0	13.3	5134	3794
30º	4.68	1.9	7.0	13.3	6123	4525
35º	4.94	1.9	7.0	13.3	6212	4590
40º	5.29	1.9	7.0	13.3	6144	4540

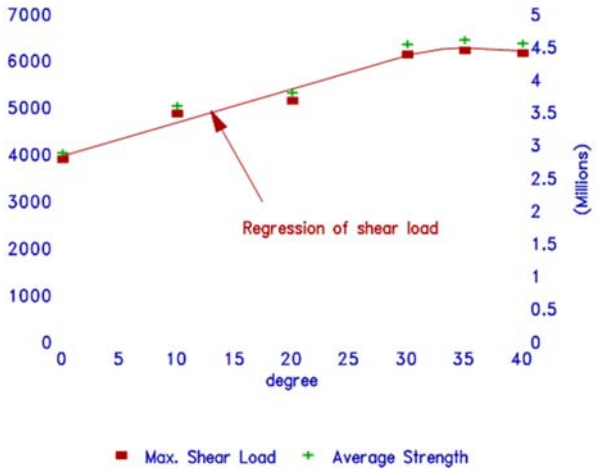

Figure-2. Failure shear load vs. slant notch degree (After [1]).

4. FINITE ELEMENT SIMULATION

For each slant notch case from 0º to 40º, a corresponding Finite Element simulation has been conducted. Eight-node PLANE82 element was used since this type of element had the singularity property. Figure 3 illustrates the entire simulation model for the 30º slant notch case with a=4.68cm. Each simulation model had the same d =1.9cm and d/H ration 0.19. The number of elements for each model varied from 3947 to 7024 and node number from 11708 to 20909 nodes.

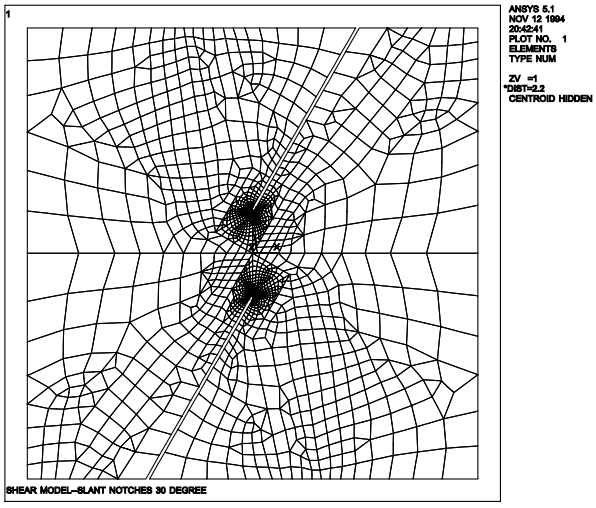

Figure-3. Simulation model for 30º slant notch case (After [1]).

The stress distributions σ_x, σ_y and τ_{xy} were determined bythe Finite Element simulations, and those stress values on half of the middle line from central point to one notch tip point are shown in Figures 4, 5, and 6, respectively. From Figures 5 and 6, it is observed that, for different specimens with different degree of inclined notches, σ_x and τ_{xy} results were almost the same along about 95 percent of the half middle line, which starts from the central point to a point notated as N with y coordinate equal to about 0.91 to 0.92cm. Only along the rest part of the middle line from N point to the notch tip point which was merely about 5 percent of the half middle line, the σ_x and τ_{xy} varied. On about 70 percent part of the half middle line, σ_y for different inclined notches were about the same, on the rest part, about 30 percent of the half middle line, the σ_y had big changes. In this study, the stress state of each point along the half middle line in terms of σ_x, σ_y and τ_{xy} were expressed in the its maximum shear stress and the corresponding sigma stress, and were plotted in the τ-σ curve. Mohr-type of power law envelope was applied on these τ-σ diagrams to evaluate the probability degree to failure of each point along the half middle line section.

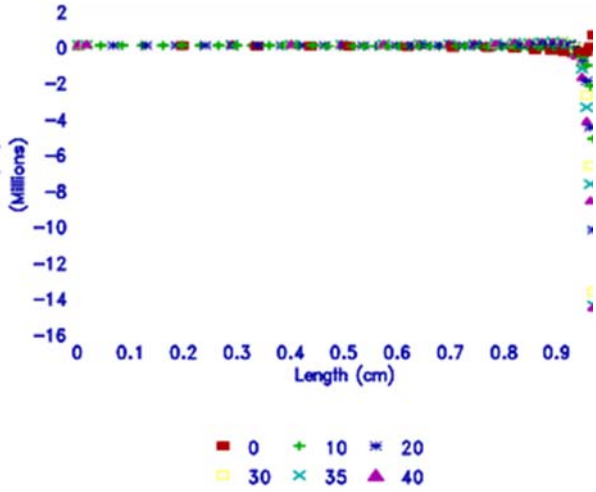

Figure-4. Stress $\sigma_x$by finite element simulations.

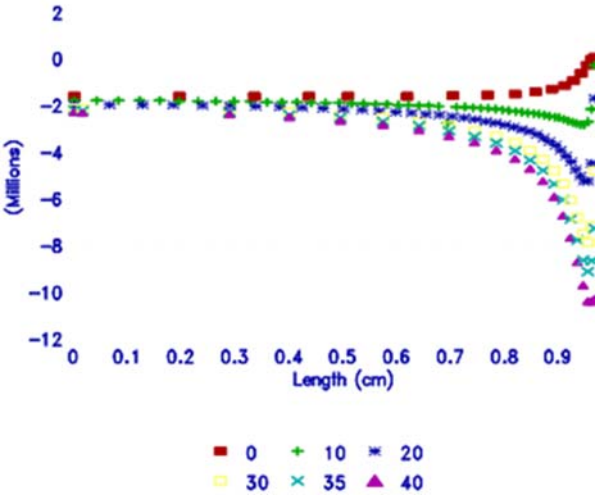

Figure-5. Stress $\sigma_y$by finite element simulations.

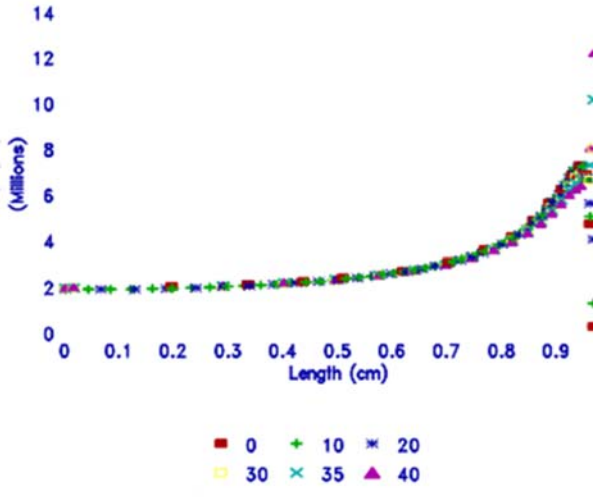

Figure-6. Shear stress τ_{xy} by finite element simulations.

5. POWER LAW FAILURE CRITERION

Mohr envelope form of power law (n-type) equation $\tau^n=a\sigma+b$ for two specific cases n = 1 which is the Coulomb (linear) case, and n = 2 were applied.
According to Pariseau [19]:

$$n = 1: a=A/[1-A^2]^{(1/2)} \text{ and } b=B/[1-A^2]^{(1/2)} \quad (1)$$

$$n = 2: a=A \text{ and } b=B+(A/2)^2 \quad (2)$$

and

$$A=\frac{(\frac{C_o}{2})^n-(\frac{T_o}{2})^n}{\frac{C_o}{2}+\frac{T_o}{2}} \text{ and } B=\frac{\frac{T_o}{2}(\frac{C_o}{2})^n+\frac{C_o}{2}(\frac{T_o}{2})^n}{\frac{C_o}{2}+\frac{T_o}{2}} \quad (3)$$

where, C_o and T_o are the uniaxial compressive and tensile strengths, respectively.

Therefore, the coefficients a and b in the Mohr envelope expression form can be derived from Equations (1) to (3) and represented in terms of the uniaxial and strengths as below:

when n = 1:

$$a=\frac{C_o-T_o}{2\sqrt{C_oT_o}} \text{ and } b=\frac{\sqrt{C_oT_o}}{2} \quad (4)$$

and when n = 2:

$$a=\frac{C_o-T_o}{2} \text{ and } b=(\frac{C_o+T_o}{4})^2 \quad (5)$$

The uniaxial compressive strength C_o of sandstone was 32.35 MPa, which was obtained experimentally as shown in Table-2 and the tensile strength T_o was 3.45 MPa [8].

Table-2. Experimental results of sandstone uniaxial compressive strength C_o.

Sample No.	Specimen Height	Section Length	Size Width	Area A	P_{max}	$C_o=P_{max}/A$	Average C_o
	h (cm)	a (cm)	b (cm)	(cm^2)	(N)	(MPa)	(MPa)
		3.8497	3.0480				32.35
1	10.08	3.9624	2.9766	11.7662	39480	33.55	
		3.6322	3.6512				
2	9.09	3.7084	3.6512	13.4010	39539	29.50	
		3.6513	3.5461				
3	9.00	3.5306	3.5306	12.7064	43192	33.99	

6. ANALYSIS AND DISCUSSION

Based on the Finite Element simulation results of σ_x, σ_y and τ_{xy}, the following equations were used to calculate σ and τ for each point along the specimen middle line:

$$\sigma=\frac{\sigma_x+\sigma_y}{2} \text{ and } \tau=\sqrt{(\frac{\sigma_x-\sigma_y}{2})^2+\tau_{xy}^2} \quad (6)$$

Figure-7 shows the stress state of each point along the half middle line in terms of τ and σ for each slant notch case from 0º to 40º under an identical load P=3883 N. In Figure-7, the tip point is notated as 1, and the subscripts a, b c, d, e and f for 0º, 10º, 20º, 30º, 35º and 40º cases respectively. The specimen central point is notated as O. It is observed from Figure-7 that, for different slant notch cases, the tip stress state changes greatly along the middle line according to the τ-σ diagram, and when the point moved from the tip point to the central point, the change on the stress state decreased, until at the central point, the stress states for different slant notches were nearly the same.

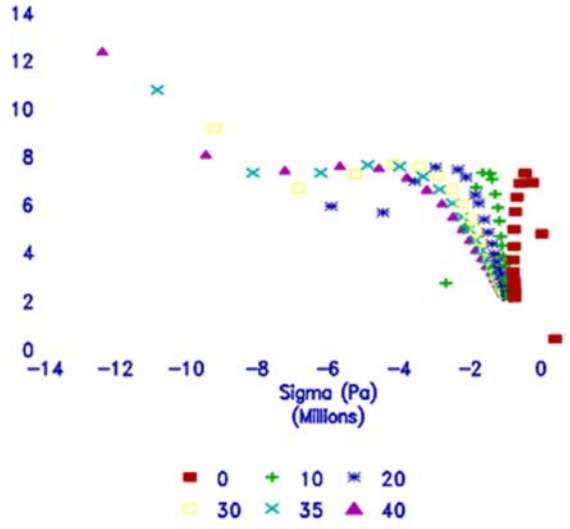

Figure-7. τ-σ curve under same load P=3883 N.

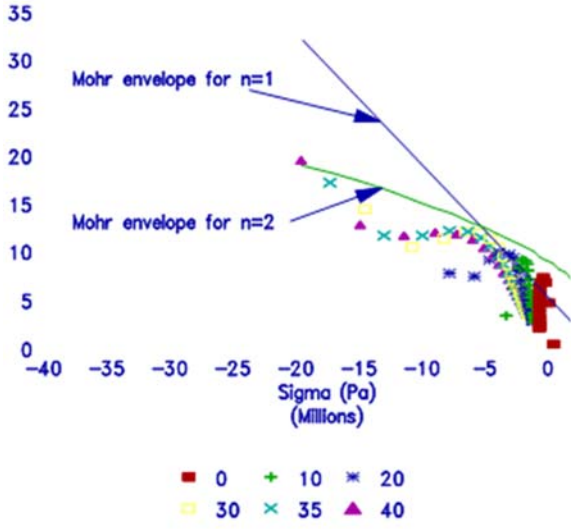

Figure-8. τ-σ curve under different load and Mohr envelopes for n = 1&n = 2.

Experimental results showed that tested sandstone specimens with different inclined notches failed under different loads (P_{max}); specimens with vertical notch failed under 3883N; specimens with 10º notch under 4851N; 20 º cases under 5134N and so on, as shown previously in Table-1 and Figure-2. For each specimen with different slant notch under its corresponding P_{max}, the τ-σ state of each point along the half middle line were calculated based on the Finite Element simulation (Figure-8). Figure-8 also displays the Mohr-type envelops for n = 1 and n = 2. Note that the sign of compression is minus, so the envelope equation for n = 1 is:

$$\tau=-\frac{C_o-T_o}{2\sqrt{C_oT_o}}\sigma+\frac{\sqrt{C_oT_o}}{2} \quad (7)$$

and for n = 2, the equation is:

$$\tau^2=-\frac{C_o-T_o}{2}\sigma+(\frac{C_o+T_o}{4})^2 \quad (8)$$

From Figure-8, it can be observed that for 30º, 35º and 40º cases, the stress state of each point along the half middle line including the tip points 1d, 1e and 1f was nearly at the same condition and bear about same probability of failure according to the Mohr envelope of n = 2, while the stress state of each point along the half middle line for 0º, 10º and 20º case was at quite different condition, and the points around the peck of the τ-σ data bear the most probability to break while the tip point and the points around the central point endure the least probability to failure according to both Mohr-type envelopes.

For specimens with vertical notch, since the tip point was in the safest state to resistant to fracture, on this case, it forced the crack propagation path to avoid the tips so a rough 'S' shape failure pattern was formed. While for specimens with 30º, 35º or 40º notch and since the tip stress state changed greatly from those for the vertical notch case and it was also in the condition to bear quite big probability to fracture, so it was ready to generate a straighter fracture path.Furthermore, the middle line stress state of specimens with 35º under 6212 N load was nearly about the same as those of specimens with 40º under 6144 N, from the view point of Mohr envelope n=2. Thus, as the notch degree increased from 35º to 40º, it is believed that the load P_{max} causing the specimen to fracture did decrease, which correspond to the experimental results as shown in Table 1 and Figure-2. In addition, from Figure 8, it was observed that the far left part of linear envelope n=1 could not fit the τ-σ data under the failure load P_{max}, while the n=2 power law equations could.

7. CONCLUSIONS AND RECOMMENDATIONS

Based on the results presented in this study, the following conclusions were made:

a) Mohr-type envelope n = 2 is better to be used to

evaluate sandstone fracture, and the far left part of linear envelope was not applicable.

b) Specimens with notch degree from 30º to 40ºwould generate a straighter crack propagation path to go through the two notch tips. The two power law envelope demonstrated the mechanism.

c) The stress state in term of τ-σ curve from Finite Element simulation results and the Mohr-type envelope could explain the reason why as the slant degree increased, the failure load increased but after 35º, the failure load decreased slightly as the notch degree increased continuously.

d) The tensile strength T_o of the sandstone was needed to have a better control to the right end of the Mohr-type envelopes, which could be used to analyze and understand more about the mechanism of the steady and curving crack propagation of the sandstone specimen with big d/H ration.

REFERENCES

[1] Jung SJ, Ba H, Whyatt, JK. 2009. Analysis of the KII Mode Shear Fracture Toughness for Brittle Materials. The 43rd US Rock Mechanics Symposium and 4th U.S.-Canada Rock Mechanics Symposium, Asheville, NC June 28th – July 1, 2009, USA.

[2] Jones DL, Chisholm DB. 1975. An Investigation of the Edge-Sliding Mode in Fracture Mechanics. Eng. Fract. Mech. 7: 261-270.

[3] Richard HA. 1981. A New Compact Shear Specimen. Int. J. of Fract. 17(5): R105-R107.

[4] Watkins J. 1983. Fracture Toughness Test for Soil-Cement Samples in Mode II. Int. J. Fract. 23: R135-R138.

[5] Huang J, Wang S. 1985. An Experimental Investigation Concerning the Comprehensive Fracture Toughness of Some Brittle Rocks. Int. J. Rock Min. Sci. and Geomech. Abstr. 22(2): 99-104.

[6] Davies J, So KW. 1986. Fracture Development of Fracture Test in Mode II Int. J. Fract. 31: R19-R21.

[7] Jung SJ, Enbaya M, Whyatt JK. 1992. The Study of Fracture of Brittle Rock under Pure Shear Loading. Research Report, University of Idaho, USA.

[8] Enbaya MM. 1991. The Dilemma of Fracture of Brittle Materials under Pure Shear Loading. Ph.D. Dissertation, University of Idaho, USA.

[9] Mahabadi O, Lisjak A, Munjiza A, Grasselli G. 2012. Y-Geo: New Combined Finite-Discrete Element Numerical Code for Geomechanical Applications. Int. J. Geomech. 12: 676-688.

[10] Eckwright F, Jung SJ, Abu Abdo AM. 2014. Utilizing a Particle Flow Code in 2 Dimensional Discrete Element Method of Fracture Resistance Evaluation of HMA and Brittle Rock. Asian Journal of Civil Engineering (BHRC). 15(1): 9-21.

[11] Wang D, Zhang Z, Ge X. 2014. Study on Shear Failure Behavior of Embedded Cracks Subjected to Different Normal Stresses. Proceedings of Geo-Shanghai: Rock Mechanics and Its Applications in Civil, Mining, and Petroleum Engineering: 79-88.

[12] Li Y, Zhou H, Zhu W, Li S, Liu J. 2015. Experimental and numerical investigations on the shear behavior of a jointed rock mass. Geosci. J., in press: 1-9. DOI 10.1007/s12303-015-0052-z.

[13] Matsui T, San KC. 1992. Finite Element Slope Stability Analysis by Shear Strength Reduction Technique. Soils Found. 32(1): 59-70.

[14] Li X. 2007. Finite element analysis of slope stability using a nonlinear failure criterion. Comput. Geotech. 34(3): 127-136.

[15] Zhao Z, Wang X. 2013. Evaluation of Potential Failure of Rock Slope at the Left Abutment of Jinsha River Bridge by Model Test and Numerical Method. Frontiers of Structural and Civil Engineering. 7(3): 332-340.

[16] Steada D, Eberhardtb E, Cogganc JS. 2006. Developments in the Characterization of Complex Rock Slope Deformation and Failure Using Numerical Modelling Techniques. Eng. Geol. 83(1-3): 217-235.

[17] Li Y, Qiao L, Sui ZL, Li QW. 2009. Strength analysis of rock material under the brittle shear failure mode. J. Cent. South Univ. T. 16(4): 663-668.

[18] Li Y, Li Z, Xu TJ. 2014. Research of Brittle Shear Failure Strength of Rock Materials. Appl. Mech. Mater. 454: 125-128.

[19] Pariseau WG. 1994. On the Significance of Dimensionless Failure Criteria. Int. J. Rock Mech. Min. Sci. and Geomech. Abstr. 31(5): 555-560.